van der Waals density functional study of CO_2 binding in zeolitic imidazolate frameworks

Keith G. Ray,[1] David Olmsted,[2] Ning He,[4] Yao Houndonougbo,[3] Brian B. Laird,[4] and Mark Asta[2]
[1]*Department of Physics, University of California, Berkeley, California, USA*
[2]*Department of Materials Science and Engineering, University of California, Berkeley, California, USA*
[3]*Department of Chemistry and Biochemistry, Eastern Washington University, Cheney, Washington, USA*
[4]*Department of Chemistry, University of Kansas, Lawrence, Kansas, USA*
(Received 30 November 2011; published 6 February 2012)

The van der Waals density functional (vdW-DF) formalism is employed in a study of the binding energetics for CO_2 in a set of five zeolitic imidazolate framework (ZIF) compounds. The ZIF structures investigated share the same RHO-type zeolite topology and metal atoms, but feature imidazolate linkers with different chemical functionalization. Three distinct binding sites are identified, for which the binding energies are found to show different dependencies on the functionalization of the linker molecules. The origin of the variations in the binding energies across the ZIF compounds is discussed through analyses of the binding geometries and charge-density distributions. A comparison of the vdW-DF results with those obtained by generalized-gradient-approximation calculations highlights the important contribution of the nonlocal correlation energy to the CO_2 binding energies in these compounds.

DOI: 10.1103/PhysRevB.85.085410 PACS number(s): 81.05.Zx, 71.15.Mb, 68.43.Bc

I. INTRODUCTION

Zeolitic imidazolate frameworks (ZIFs) are a class of metal-organic-framework compounds that have received widespread interest for applications involving capture, storage, and separation of molecular gas species.[1–6] As illustrated in Fig. 1, for the example of ZIF-96, the structures of ZIF compounds are characterized by a tetrahedral coordination of the metal ions to the nitrogen atoms on the imidazole organic linker molecules. The geometry of the linkers dictates that the bond angle between the metal ions is close to 145 degrees, which is similar to that associated with the Si-O-Si bonds connecting SiO_4 tetrahedra in zeolite compounds. Consequently, ZIFs are observed to assemble in many of the same topologies as zeolites. Experimental efforts over the past five years have demonstrated that ZIF compounds can be formed with a range of structural topologies and compositions. ZIFs have been synthesized using different metal ions (e.g., Co and Zn), and with linkers featuring a variety of different functional groups, which can be attached to the 2 or 4 and 5 sites of the imidazole ring.[1]

Due to the wide variety of possible topological and compositional variations, a detailed understanding of the factors that govern gas adsorption is desired to guide optimization of ZIF compounds for gas storage and separation applications. Experimental measurements have demonstrated a pronounced dependence on ZIF chemical compositions and structural topologies, for the equilibrium adsorptions of H_2, CO_2, CH_4, N_2, and CO gases and their mixtures.[1,7–11] Neutron-scattering, spectroscopy measurements, and Monte Carlo computer simulations[12–14] have provided important insights related to these results by demonstrating that the gas molecules bind primarily in sites localized near the atoms in the imidazolate linkers in ZIF compounds.[8,13,15–27] The magnitudes of the binding energies underlying the interactions between the gas species and ZIF linkers can be estimated based on the measured isosteric heat of adsorption [e.g., 0.24 eV (23 kJ mol^{-1}) for CO_2 in ZIF-69, Ref. 10].

The interactions between gas and linker molecules in ZIF compounds have been investigated theoretically for a few ZIFs using quantum-chemistry methods. Focusing specifically on the case of CO_2 molecules, of interest in the present study, the nature of these interactions has been investigated for isolated fragments of the 2-nitrobenzimidazolate (nbIM) and methylbenzimidazolate (MebIM) linkers in ZIF-78 and ZIF-79 (Ref. 23), and for embedded clusters involving the benzimidazolate (bIM), nbIM, and 5-chlorobenzimidazolate (cbIM) linkers in ZIF-68 and ZIF-69 (Ref. 22). In Ref. 23, binding energies ranging between −0.0518 eV (−5.00 kJ mol^{-1}) and −0.1371 eV (−13.23 kJ mol^{-1}) were obtained. The geometries of the strongest binding sites in these studies involved two types of interactions. In the first the C atom in CO_2 is located at distances 2.8 to 3.15 Å from the O atoms in the $-NO_2$ groups on the nbIM linkers, or the N atoms in the imidazole ring. The second involved hydrogen bonds between the O atoms in CO_2 and H atoms attached to the benzene ring.

In the current work we employ the framework of the van der Waals density functional (vdW-DF)[28,29] in a computational study of the energetics of CO_2 binding in the set of five ZIF compounds illustrated in Fig. 1. These compounds are referred to as ZIF-25, ZIF-71, ZIF-93, ZIF-96, and ZIF-97, and are described in detail in Ref. 8. These ZIFs share the same RHO-type zeolite topology, and differ only in the nature of the functional groups attached to the 4 and 5 sites of the imidazole linkers (see Sec. III). The RHO-type net consists of a BCC arrangement of truncated cuboctohedra along with smaller space filling polyhedra, see Fig. 1(c). In a previous experimental and computational study of CO_2 uptakes in these compounds,[8] the measured adsorptions were shown to vary by a factor of 3.3 at 298 K and a gas pressure of 103 kPa. Additionally, Monte Carlo simulations based on classical force fields were used to identify the main binding sites and established the importance of electrostatic interactions for compounds featuring asymmetric linkers (i.e., different functional groups on the 4 and 5 sites of the imidazole ring). Due to the variation in equilibrium adsorptions displayed by

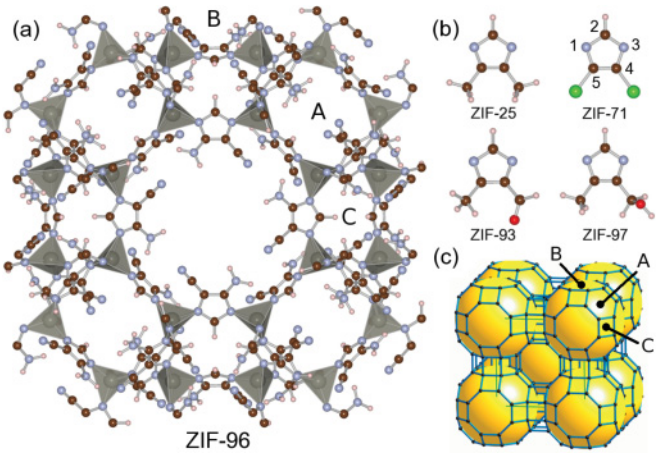

FIG. 1. (Color) Structure of the RHO-topology ZIFs considered in this work, with important binding sites *A*, *B*, *C* labeled. Purple spheres are nitrogen, red are oxygen, brown are carbon, green are chlorine, light rose are hydrogen, and the grey tetrahedra are centered on the zinc atoms. (a) ZIF-96 as an example, viewed along the [100] direction. The functional groups in ZIF-96 are $-NH_2$ and $-CN$. (b) The structure and composition (functional groups in parentheses) of the linkers in ZIF-25 ($-CH_3$), ZIF-71 ($-Cl$), ZIF-93 ($-CH_3$, $-CHO$), and ZIF-97 ($-CH_3$, $-CH_2OH$). Imidazolate site labels are given for ZIF-71. (c) A representation of the BCC periodic structure of zeolite RHO topology, where vertices correspond to zinc positions, and the large yellow spheres represent the size of the pores within the framework.

these compounds, and the fact that they differ only in the composition of their linkers, they represent an ideal set of structures for probing the nature of CO_2 interactions with ZIF framework atoms, and the ways in which these interactions can be altered through variations in linker chemistry.

In the next section we describe the approach employed in the present work, based on the use of the vdW-DF. This approach offers a methodology within density functional theory (DFT) for incorporating nonlocal correlation contributions to the total energy, which are known to be critical for accurately modeling nonbonded interactions in molecules and solids.[28–31] Due to relatively recent algorithmic developments,[32] vdW-DF calculations can be performed with a computational expense only moderately increased relative to standard DFT methods. The vdW-DF formalism is thus well suited to studies of gas binding in metal-organic-framework materials such as ZIFs.[33–35] Specifically, the formalism allows one to perform direct calculations of gas binding energies in fully periodic structures, incorporating in a natural way simultaneous interactions with multiple linkers (e.g., in small apertures), and the steric constraints imposed by the topology of the framework. After describing the details of the computational approach, the results from DFT are presented and compared with those obtained from classical force fields in Sec. III. An analysis of the binding geometries and energies is given in Sec. IV. A short summary of the main conclusions is given in Sec. V.

II. METHODS

The computational approach employed in this work involves a combination of classical force field (FF) and vdW-DF calculations. The former are used to map the potential energy landscape of the CO_2 molecule within the unit cell of the ZIF compound. The most stable binding geometries identified from these calculations are then used as a starting point for vdW-DF calculations in which the positions of the atoms in the CO_2 molecule are relaxed to a local minimum. The framework atomic positions are taken from the experiment[8] and remain fixed. The remainder of this section describes the details surrounding both the classical force-field and vdW-DF calculations.

A. Classical simulations

The classical simulations employed in this work were used to map out the potential energy landscape of a single CO_2 molecule within the ZIF framework, as a function of the position of its center of mass, and its angular orientation. The calculations employed force fields including van der Waals interactions modeled with Lennard-Jones potentials and electrostatic interactions modeled through the assignment of partial charges on each of the atoms. The Lennard-Jones potential parameters and partial charges for CO_2 were taken from the elementary physical model 2 (EPM2) force field of Harris and Yung.[36] For the framework atoms the Lennard-Jones parameters were taken from the optimized potentials for liquid simulations (OPLS) set[37] that most closely represented the chemical coordination of the functional groups. Lennard-Jones parameters between CO_2 and the framework atoms were derived using Lorentz-Berthelot mixing rules.[38] Partial charges for the framework atoms were derived from electrostatic potentials, computed from Perdew-Burke-Ernzerhof (PBE)[39] generalized gradient approximation (GGA) DFT calculations, using the repeating electrostatic potential extracted atomic (REPEAT) charges algorithm,[40] as described in detail in the supplementary material to Ref. 8.

Energies for a single molecule in a single cubic unit cell of the ZIF compound were computed using the large-scale atomic/molecular massively parallel simulator (LAMMPS) molecular-dynamics code[41] with charge interactions summed using a particle-mesh Ewald (PPPM) technique.[42] Appropriate energies for the ZIF and molecule alone were subtracted to compute binding energies. The binding energies were computed sampling the center-of-mass position of the CO_2 molecule on a rectangular grid with steps $L/128$, where L is the length of a side of the cubic unit cell. The symmetries of the ZIF structure were used to reduce the number of actual computations. CO_2 was treated as a linear rigid molecule and energies were computed for 61 orientations at each center-of-mass position. These consisted of all the $\langle 100\rangle$, $\langle 110\rangle$, $\langle 111\rangle$, $\langle 321\rangle$, $\langle 2.414\ 1\ 0\rangle$, and $\langle 2.732\ 1\ 1\rangle$ directions over the half-sphere. The results plotted in Fig. 2 represent the minimum energies over these 61 orientations, for each center-of-mass position.

B. van der Waals DF calculations

For the three most stable binding sites obtained from the classical simulations described above, we undertake calculations of CO_2 binding energies employing the formalism of the vdW-DF.[28] In this formalism, the vdW contribution to

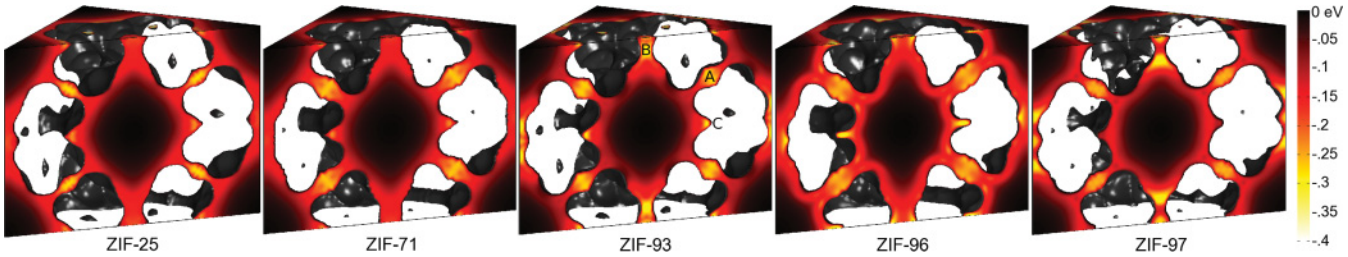

FIG. 2. (Color online) CO_2 binding energies derived from classical force fields are plotted as a function of the center-of-mass position within the five RHO-topology ZIFs considered in this work. The slice corresponds to a (110) plane centered on the middle of the pore for each unit cell. The three dominant binding sites, common to each structure, are labeled *A*, *B*, and *C* on the plot for ZIF-93. The positions of the same three points are also labeled on Fig. 1 to reference the positions in this figure to the atomic sites.

the total energy is described through modifications to the correlation energy functional within DFT. Specifically, the DFT exchange-correlation functional is divided into three parts

$$E_{xc} = E_{lc} + E_{nlc} + E_x, \tag{1}$$

where E_{lc} is a local correlation energy described within the local density approximation, E_{nlc} is the nonlocal correlation energy, and E_x is a semilocal exchange functional. The E_{nlc} contribution is given by the integral

$$E_{nlc} = \frac{1}{2}\int d\mathbf{r}d\mathbf{r}'n(\mathbf{r})\phi(\mathbf{r},\mathbf{r}')n(\mathbf{r}'), \tag{2}$$

over electron densities, n at $\mathbf{r}$ and $\mathbf{r}'$, multiplied by an integration kernel ϕ, which is derived from the adiabatic-connection theorem through a series of approximations.[28] We consider three different exchange functionals for use with the vdW-DF approach, as proposed previously in the literature.[28–31] These are revPBE,[43] as in the original vdW-DF,[28] PW86,[44] as in vdW-DF2,[29] and optB88,[30] a new exchange functional based on the B88 exchange functional.[45] E_{nlc} in the original vdW-DF and the optB88 formulation are based on the same parametrization. By contrast, E_{nlc} in vdW-DF2 has a single changed parameter, which relates how the length scale in E_{nlc} is set by a corresponding GGA calculation. In vdW-DF2 and vdW-DF this parameter comes from energy expansions appropriate for molecules or a slowly varying electron gas, respectively. The PW86 and optB88 functionals were shown to be the most accurate for the S22 data set of dispersion bound molecular complexes.[29,30] In what follows we use the vdW-DF2 functional in calculating binding energies for all five ZIFs listed in Fig. 1. For comparison purposes, we also present results using the vdW-DF, optB88, and PBE-GGA[39] functionals for ZIF-25 and ZIF-96.

The PBE and vdW-DF calculations were performed using the Vienna Ab Initio Simulation Package (VASP)[46] with the vdW-DF implementation due to Jiří Klimeš.[31] The projector-augmented wave (PAW) scheme[47] is utilized with the potentials taken from the VASP PBE library. The electronic wave functions were expanded in a plane wave basis with a cutoff of 550 eV. A single k-point (Γ) was found to be sufficient to sample the Brillouin zone due to the large size of the ZIF unit cell. In the calculations, the position, bond lengths and bond angles of the CO_2 molecule were optimized with a convergence criteria for the forces of 0.01 eV/Å. With these parameters, binding energies are estimated to be converged to better than 2 meV.

III. RESULTS

The five ZIF compounds considered in this work share the same RHO topology, illustrated in Fig. 1, and feature Zn ions coordinated to the following linkers: $C_5H_8N_2$ **dmeIm** (ZIF-25), $C_3H_2N_2Cl_2$ **dcIm** (ZIF-71), $C_5H_6N_2O$ **aImeIm** (ZIF-93), $C_4H_4N_4$ **cyamIm** (ZIF-96), and $C_5H_8N_2O$ **hymeIm** (ZIF-97). These linkers feature the following functionalizations on the 4, 5 sites of the imidazole ring: two $-CH_3$ groups (ZIF-25), two $-Cl$ atoms (ZIF-71), one $-CHO$ and one $-CH_3$ group (ZIF-93), one $-CN$ and one $-NH_2$ group (ZIF-96), and one $-CH_2OH$ and one $-CH_3$ group (ZIF-97).

The results of the classical force-field calculations of potential-energy landscapes are shown in Fig. 2. This figure plots the binding energies of a single CO_2 molecule, minimized with respect to angular orientation, as a function of the center-of-mass position. The results illustrate that there are three main binding sites common to each of the ZIF structures. These sites are labeled *A*, *B*, and *C* in the middle panel of Fig. 2. The same sites are also labeled in Figs. 1(a) and 1(c) to establish the relationship between the plots in Fig. 2 and the framework atoms.

Site *A* lies in the hexagonal connection between the large Linde-type A (*lta*) pores along the ⟨111⟩ direction from the center of the pore in Fig. 1. This site is surrounded by a six-fold ring of Zn ions connected by six linkers. Site *B* lies in the bridging double eight-fold rings (*d8r*) connecting the pores along the ⟨100⟩ direction. Site *C* corresponds to a binding site on the inner surface of the pore along the ⟨110⟩ direction near the four-fold zinc ring [see Figs. 1(a) and 1(c)]. The multiplicity of these binding sites per primitive unit cell is *A*: 4, *B*: 3, *C*: 12.

In Fig. 2 it is apparent that the strength of the binding energies for site *A* is fairly constant across the different structures, with a value of approximately −0.3 eV predicted by the classical force field. By contrast, larger variations are seen for the strength of the binding in sites *B* and *C*. Specifically, sites *B* and *C* show the weakest binding in ZIF-71 (−0.19 eV) and ZIF-97 (−0.15 eV), respectively, and the strongest binding in ZIF-96 (−0.31 eV for site *B* and −0.34 eV for site *C*). These variations in binding energies in sites *B* and *C* correlate with

TABLE I. A comparison of CO_2 binding energies (in eV) calculated with classical force-fields (FF), PBE, and three different vdW-DF methods. Results are listed for each of the three binding sites *A*, *B*, and *C* in ZIF-25 and ZIF-96.

ZIF	Site	FF	PBE	vdW-DF	vdW-DF2	vdW-optB88
25	*A*	−0.299	−0.090	−0.461	−0.419	−0.463
	B	−0.210	−0.047	−0.329	−0.235	−0.272
	C	−0.254	−0.053	−0.359	−0.319	−0.367
96	*A*	−0.286	−0.039	−0.467	−0.376	−0.440
	B	−0.306	−0.105	−0.401	−0.385	−0.433
	C	−0.342	−0.134	−0.388	−0.434	−0.475

TABLE II. CO_2 binding energies (in eV) calculated by vdW-DF2 for binding sites *A*, *B*, and *C* in five RHO-structured ZIFs. The contribution of the nonlocal correlation (*nlc*) energy to the binding energy is listed in parentheses.

ZIF	Site *A* total (*nlc*)	Site *B* total (*nlc*)	Site *C* total (*nlc*)
25	−0.419 (−0.437)	−0.235 (−0.275)	−0.319 (−0.430)
71	−0.413 (−0.469)	−0.323 (−0.367)	−0.310 (−0.393)
93	−0.373 (−0.465)	−0.408 (−0.282)	−0.433 (−0.469)
96	−0.376 (−0.444)	−0.385 (−0.393)	−0.434 (−0.449)
97	−0.460 (−0.465)	−0.464 (−0.268)	−0.250 (−0.219)

the fact that ZIF-71 and ZIF-97 show the lowest two measured CO_2 adsorptions, while ZIF-96 shows the highest.[8]

In Table I classical FF, PBE, and vdW-DF calculated results are listed for the binding energies in sites *A*, *B*, and *C* in ZIF-25 and ZIF-96. The PBE binding energies are considerably smaller in magnitude than the binding energies derived from the vdW-DFs, as well as the classical force fields. Given that the classical models produce adsorption values in reasonable agreement with measurements, the PBE functional significantly underestimates the strength of the binding energy for the CO_2 molecules in the ZIF frameworks. This result is not surprising given that the dispersion contributions to the nonbonded interactions are not properly accounted for in this functional. The vdW-DF methods are seen to lead to significantly larger magnitudes for the binding energies than PBE. The differences between PBE and vdW-DF results can be viewed as a manifestation of the sizable contributions arising from the nonlocal correlation energy in the latter formalism.

The vdW-DF binding energies in Table I are generally larger in magnitude than the values obtained with the classical FFs. This general trend is also observed in a comparison of vdW-DF and FF results for the three binding sites in the three other RHO-structured ZIF compounds considered in this work (71, 93, and 97). The reason for this trend may be partly due to polarization effects which are not explicitly accounted for in the classical FF results. For example, we note that the vdW-DF2 results for the *B* site show relatively small differences with the FF results in ZIF-25, while the differences are much larger for this site in ZIF-96. As shown in the next section, the charge density redistribution on the functional groups induced by the CO_2 molecule are much larger in magnitude for ZIF-96 than for ZIF-25. Thus, the explicit inclusion of polarization terms in the classical FFs may be required to accurately reproduce the magnitudes of the binding energies, and associated variations across the different compounds, obtained by the vdW-DF calculations.

The differences between the binding energies obtained with the different vdW density functionals in Table I are largely consistent with trends reported previously in the literature. Specifically, the original vdW-DF is known to overbind at greater than equilibrium separations for dispersion bound systems and predict equilibrium bond lengths that are too large for such systems.[28–30] The vdW-DF2 method was designed to improve the method in both regards.[29] Most of the vdW-DF results in Table I show larger binding energies relative to vdW-DF2. One exception is the *C* site in ZIF-96; the smaller magnitude of the binding energy for this site predicted by vdW-DF relative to vdW-DF2 may be due to the larger bond lengths predicted in the former functional and the possibility that the bonding geometry is more optimally satisfied for the latter. For completeness, we also include in Table I results for the recently developed vdW-optB88 functional.[30] This functional yields magnitudes for the binding energies that are uniformly larger than vdW-DF2, and in some cases larger than those obtained with vdW-DF.

Overall, the results in Table I show a relatively large variation (by as much as 0.09 eV) in the binding energies predicted by the different vdW-DF theories, and also highlight the significantly larger magnitudes of the vdW-DF binding energies relative to those obtained with the classical FF (as large as 0.12 eV). Unfortunately, the available experimental data for CO_2 adsorption in the RHO-structured ZIF compounds considered here[8] do not provide a basis for direct comparisons with the results presented in Table I. Thus, to better assess the relative accuracy of the different vdW-DF formalisms in their application to CO_2 adsorption in the ZIF compounds studied here and the performance of the classical FFs, direct experimental measurements of binding energies and/or vibrational frequencies would be particularly useful. In the remainder of this paper we will focus on results obtained with the vdW-DF2 method. The main emphasis in what follows will be the trends in the energetics across the different compounds and the nature of the interactions underlying CO_2 binding.

Calculated binding energies, obtained with the vdW-DF2 formalism, are listed in Table II for the three major binding sites in ZIF-25, 71, 93, 96, and 97. Consistent with the results obtained with the classical force fields, the binding energies for the *A* site show relatively small variations across the five ZIF compounds: these energies vary by approximately ten percent about the mean value of −0.41 eV. By contrast the binding energies for sites *B* and *C* show variations in the range of 0.2 eV across the different compounds. For site *B* the magnitude of the binding energy is significantly larger for the three ZIFs (93, 96, and 97) featuring linkers with asymmetric functionalizations (i.e., two different functional groups on the 4 and 5 sites). For site *C* this trend is also observed, but with the exception of ZIF-97 which features the binding energy with the smallest magnitude. In the next section we discuss the origins of the variations in the binding energies listed in Table II through analyses of the binding geometries,

the dispersion contributions to the interaction energies, and the electronic charge distributions.

IV. DISCUSSION

We consider first site *A*, for which the binding energy shows the least variation between the five ZIF compounds. Figure 3 shows the configuration of the CO_2 molecule in this binding site for the example of ZIF-71. The molecule is positioned near the center of this site, allowing it to interact with all six nearby linkers. The closest neighbors to the CO_2 molecule are the carbon atoms at the 4 and 5 sites in the imidazole ring, which are located at a distance of 3.3 Å from an oxygen in CO_2 (the chlorine atoms are found at larger distances). This trend is similar for site *A* for the other four ZIFs as well: the CO_2 molecule in all cases is positioned such that its closest neighbors are within the imidazole rings, and such that its coordination with these neighbors is maximized. The relatively small variation in the binding energies in site *A* across the compounds is consistent with the similarity of the binding geometries, and the fact that

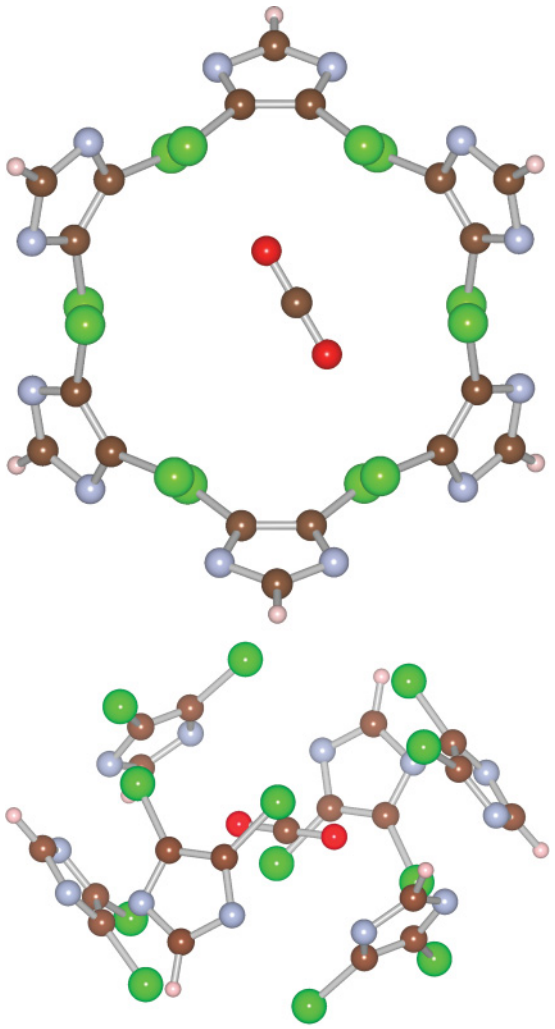

FIG. 3. (Color online) The position of the CO_2 molecule in binding site *A* of ZIF-71 is shown in relation to the six nearest **dcIm** imdazole linkers in a view along the [111] direction (top) and in a view along a direction slightly rotated out of the (100) plane (bottom).

the primary interactions (i.e., closest neighbor distances) are with the atoms in the imidazole ring, rather than the functional groups attached to these rings. An analysis of the electronic charge redistribution shows relatively little polarization of the neighboring framework atoms by the CO_2 molecule in site *A* (as compared to sites *B* and *C* discussed below), such that the interactions are interpreted to be largely dispersive in nature. This interpretation is consistent with the fact that the binding energies calculated for the *A* site show the largest differences between the PBE and the vdW-DF method in Table I, given that van der Waals contributions to nonbonded interactions are known to be significantly underestimated by PBE.

The binding energies in site *B* show the largest variation between the ZIF compounds. In contrast to site *A*, the CO_2 molecule is positioned most closely to the atoms in the functional groups on the linkers in site *B*. The binding geometries and the electronic charge density redistributions associated with site *B* are shown in Fig. 4. (The charge density redistributions plotted in Fig. 4 are defined as the difference between the self-consistent charge density with the CO_2 molecule present in the ZIF, and the sum of the charge densities of the ZIF compound and an isolated CO_2 molecule.) The closest neighbors to the atoms in the CO_2 molecule are all at distances of at least 2.7 Å, with the exception of ZIF-96, where the oxygen atoms in CO_2 are positioned 2.2 Å from the H atoms in the $-NH_2$ functional groups. The site-*B* binding geometry in ZIF-25 and ZIF-71 is influenced by the symmetric nature of the linkers (i.e., the fact that the functional groups on sites 4 and 5 are identical in these structures). This gives rise to a symmetric positioning of the CO_2 molecule relative to the functional groups. Dipole moments are induced on the functional groups pointing away from (toward) the positively (negatively) charged C (O) atoms of the CO_2 molecule. ZIF-93 and ZIF-97 show very similar binding geometries, which are characterized by a pronounced polarization of the CO_2 molecule. Both ZIF-93 and −97 feature asymmetric linkers that contain one $-CH_3$ functional group, which is seen to show minimal polarization. By contrast, polarization of the alternate functional group, −CHO in ZIF-93 and $-CH_2OH$ in ZIF-97, is more pronounced and its proximity to the carbon in CO_2 is consistent with a favorable electrostatic interaction. In both ZIF-93 and ZIF-97 the center-of-mass position of the CO_2 molecule is shifted so that one of its oxygen atoms, with the larger induced electron density, is positioned away from the ring and toward the center of the pore. The binding geometry in ZIF-96 is seen to be much more complex, and features interactions between the −CN functional group nitrogen and the carbon atom in the CO_2 molecule at a distance of 3.2 Å, as well as between the oxygen atoms in the CO_2 and the hydrogen atoms in $-NH_2$ which form hydrogen bonds at a distance of 2.2 Å.

A representative binding geometry for site *C* is shown in Fig. 5 for the case of ZIF-96. This site features a positioning of the CO_2 molecule such that it is located near the hydrogen atoms attached to the 2-site carbon atoms on four linkers, and near one of the two functional groups on four other linkers; in the ZIF structures with asymmetric linkers the four neighboring functional groups are two of each type. Thus, the binding geometry in this site shows a behavior intermediate between sites *A* and *B*, where the primary interactions are

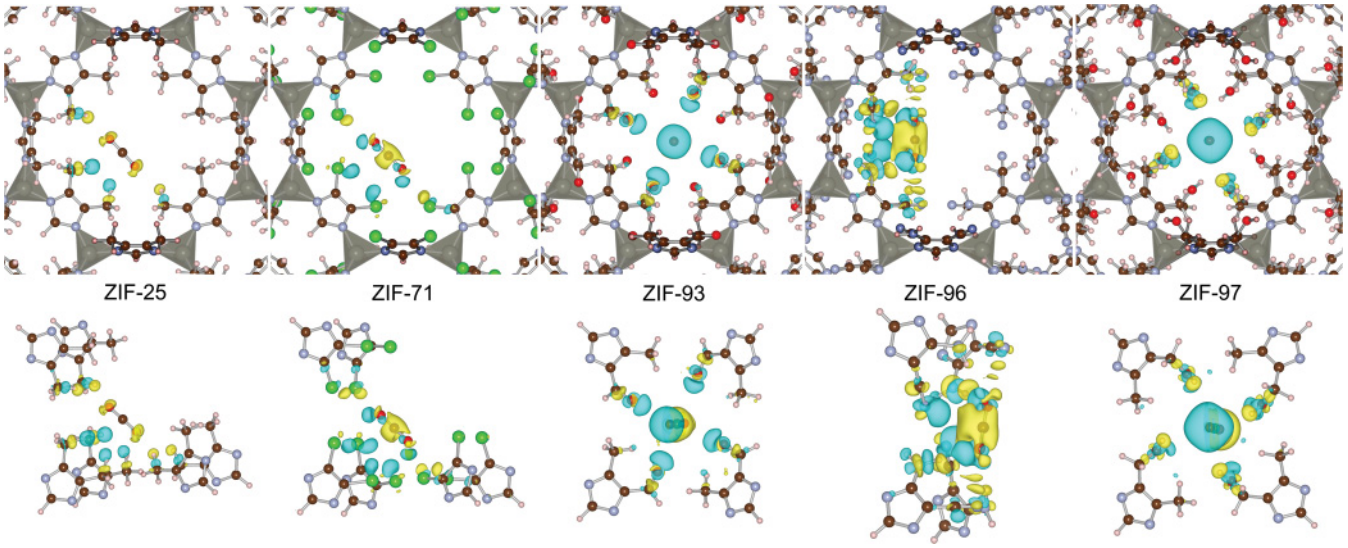

FIG. 4. (Color) Charge redistribution induced by the presence of the CO_2 molecule in binding site B for ZIF-25, 71, 93, 96, and 97. In the upper panels the the entire framework is shown. In the lower panels only the neighboring linkers that display significant polarization are shown. The yellow and blue isosurfaces denote a charge density of -0.001 e/Å^3 and $+0.001$ e/Å^3, respectively, where e is negative, indicating regions which lost and gained electrons. Purple spheres are nitrogen, red are oxygen, brown are carbon, green are chlorine, light rose are hydrogen, and the grey tetrahedra are centered on the zinc atoms.

with the imidazole and functional group atoms, respectively. For all of the ZIF compounds except ZIF-97, the closest neighbor distances are between the oxygen atoms in CO_2 and the hydrogen atoms on the 2-site of the imidazole ring: these neighboring atoms feature bond lengths of 2.45 Å in ZIF-96 and ZIF-71, 2.32 Å in ZIF-93 and 2.68 Å in ZIF-25. The magnitude of the binding energy is largest in the asymmetrically functionalized ZIF-93 and ZIF-96 structures. In these structures the positively charged carbon atom in CO_2 is positioned close to the negatively charged atoms in the functional groups. Specifically the CO_2 carbon is located at a distance of 2.9 Å from the oxygen atom in the $-$CHO group in ZIF-93, and 2.8 Å from the nitrogen atom in the $-$CN group in ZIF-96. The weakest binding energy for site C is found for ZIF-97. In this structure the CO_2 molecule is found to be positioned further out into the pore, relative to the other compounds, minimizing the types of interactions with the linker atoms described above for ZIF-93 and ZIF-96. This may reflect steric hindrance caused by the large size of the $-CH_2OH$ groups in ZIF-97.

We turn finally to an analysis of the role of the nonlocal-correlation (nlc) contribution to the binding energies calculated in the vdW-DF formalism. This contribution underlies the large differences between the PBE and vdW-DF results listed in Table I, and the variations in this term across the ZIFs can be used as a measure of the variations in the strength of the dispersion interactions underlying CO_2 binding with the framework atoms. The nlc contribution to the binding energy is defined by the double integral given in Eq. (2), which reduces to the asymptotic $1/R^6$ form at large distances.[28] The magnitudes of the nlc contributions to the binding energies are given in parentheses next to the total values in Table II. In general, this contribution is seen to be large, with magnitudes that are comparable to or even larger than the total binding energy. The value of the nlc energy contribution varies by only 0.032 eV in the A site across the five ZIF compounds. By contrast, in the B and C sites this contribution shows much larger variations of 0.125 and 0.250 eV, respectively.

Focusing on site B, the trends in the values of the nlc contribution to the binding energy across the ZIFs can be rationalized by interpreting this term as being dominated by the dispersion interactions between the CO_2 and the functional groups on the linkers. The dispersion interactions between two atoms or molecules can be approximated through the generalized Casimir-Polder formula[48–50]

$$E_{AB}^{\text{disp}} \approx -\frac{C_6}{R^6}, \tag{3}$$

$$C_6 = \frac{3}{\pi}\int_0^\infty \alpha^A(iw)\alpha^B(iw)dw, \tag{4}$$

where R is the intermolecular distance and α is the frequency-dependent dipole polarizability. Due to the rapid decay of this energy with respect to distance, and the nature of the binding geometries of the B site discussed above, the largest dispersion interactions are expected to be between the CO_2 molecule and the atoms in the closest neighboring functional groups. Thus, the coordination and polarizability of these groups are expected to be the key factors governing the magnitude of the dispersion interactions in this site. We define the coordination in site B by the number of functional groups at a distance less than 3.5 Å from the CO_2 molecule. The coordination number for the binding geometries in ZIF-25, 71, and 96 is 8, while in ZIF-93 and ZIF-97 it is 4. Thus, we expect the dispersion interactions to be larger in the former three ZIFs assuming similar polarizabilities. However, the $-CH_3$ groups in ZIF-25 have a smaller polarizability than the functional groups for the other ZIFs with the CO_2 sharing the same coordination, namely, the $-$Cl atom in ZIF-71 and the $-NH_2$ and $-$CN groups in ZIF-96. Thus, the total contribution from dispersion

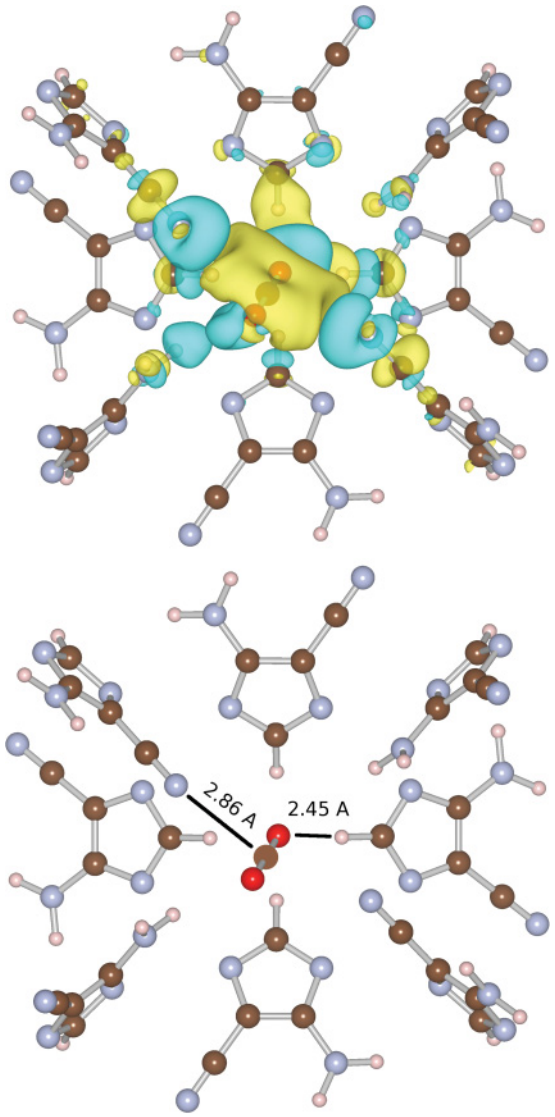

FIG. 5. (Color) The position of the CO_2 in binding site *C* of ZIF-96 is shown in relation to the nearest **cyamIm** imdazole linkers. The charge density redistribution is plotted using the same thresholds as in Fig. 4 and relevant C–N and O–H distances are indicated in Å.

interactions should be relatively smaller in ZIF-25. With this reasoning we can rationalize the trend

$$E_{96}^{\text{disp}}, E_{71}^{\text{disp}} > E_{25}^{\text{disp}}, E_{93}^{\text{disp}}, E_{97}^{\text{disp}} \quad (5)$$

shown for the *nlc* contribution in the *B* site in Table II.

V. SUMMARY AND CONCLUSION

The formalism of the vdW-DF has been used to compute the binding energies of CO_2 in five ZIF compounds featuring the same zeolite-RHO topology, but different functionalizations of the imidazole linkers. A comparison of the vdW-DF results with similar calculations performed using PBE highlights the important role of the nonlocal correlation energy in governing the binding energies in these systems, and points to the significance of the dispersive contributions to the interactions between CO_2 and framework atoms in these compounds.

Results are presented for the three dominant binding sites labeled *A*, *B*, and *C* in Figs. 1 and 2. Site *A* shows the least variation in the calculated binding energies across the different compounds, consistent with a binding geometry featuring shortest neighbor distances between CO_2 and the atoms in the imidazole ring. Site *B* displays the largest variation in binding energies, consistent with binding geometries featuring dominant interactions between the CO_2 molecule and the atoms in the functional groups attached to the linkers. In site *C* the binding is intermediate in behavior, featuring comparable neighbor distances between CO_2 and atoms in both the imidazole ring and the functional groups.

From an analysis of the bond lengths, electronic charge redistribution, and contributions from nonlocal correlation energy, we conclude that CO_2 binding in the ZIF compounds studied in this work is governed by a combination of electrostatic, dispersive, and hydrogen-bonding interactions. The vdW-DF calculations suggest that these contributions work in a delicate balance to produce a variety of binding behavior that can be optimized through changes in the functionalization of the linker molecules, and that should be sensitive to changes in the framework topology as well.

ACKNOWLEDGMENTS

We would like to thank William Morris and Colin Ophus for valuable discussions and for their assistance with the figures. Figure 1(c) was reproduced from William Morris, with his permission. This work was supported as part of the Molecularly Engineered Energy Materials, an Energy Frontier Research Center funded by the US Department of Energy, Office of Science, Office of Basic Energy Sciences under Award No. DE-SC0001342. This work made use of resources of the National Energy Research Scientific Computing Center, supported by the Office of Science of the US Department of Energy under Contract No. DE-AC02-05CH11231.

[1] A. Phan, C. J. Doonan, F. J. Uribe-Romo, C. B. Knobler, M. O'Keeffe, and O. M. Yaghi, Acc. Chem. Res. **43**, 58 (2010).

[2] H. Hayashi, A. P. Cote, H. Furukawa, M. O'Keeffe, and O. M. Yaghi, Nat. Mater. **6**, 501 (2007).

[3] S. R. Venna and M. A. Carreon, J. Amer. Chem. Soc. **132**, 76 (2010).

[4] K. S. Park, Z. Ni, A. P. Côté, J. Y. Choi, R. Huang, F. J. Uribe-Romo, H. K. Chae, M. O'Keeffe, and O. M. Yaghi, Proc. Natl. Acad. Sci. **103**, 10186 (2006).

[5] X.-C. Huang, Y.-Y. Lin, J.-P. Zhang, and X.-M. Chen, Angewandte Chemie International Edition **45**, 1557 (2006).

[6] R. Banerjee, A. Phan, B. Wang, C. Knobler, H. Furukawa, M. O'Keeffe, and O. M. Yaghi, Science **319**, 939 (2008).

[7]S. Aguado, G. Bergeret, M. P. Titus, V. Moizan, C. Nieto-Draghi, N. Bats, and D. Farrusseng, New J. Chem. **35**, 546 (2011).
[8]W. Morris, B. Leung, H. Furukawa, O. K. Yaghi, N. He, H. Hayashi, Y. Houndonougbo, M. Asta, B. B. Laird, and O. M. Yaghi, J. Amer. Chem. Soc. **132**, 11006 (2010).
[9]Y. Li, F. Liang, H. Bux, W. Yang, and J. Caro, J. Membrane Science **354**, 48 (2010).
[10]J. Pérez-Pellitero, H. Amrouche, F. Siperstein, G. Pirngruber, C. Nieto-Draghi, G. Chaplais, A. Simon-Masseron, D. Bazer-Bachi, D. Peralta, and N. Bats, Chemistry – A European Journal **16**, 1560 (2010).
[11]H. Huang, W. Zhang, D. Liu, B. Liu, G. Chen, and C. Zhong, Chemical Engineering Science **66**, 6297 (2011).
[12]H. Amrouche, S. Aguado, J. Pérez-Pellitero, C. Chizallet, F. Siperstein, D. Farrusseng, N. Bats, and C. Nieto-Draghi, J. Phys. Chem. C **115**, 16425 (2011).
[13]B. Assfour, S. Leoni, S. Yurchenko, and G. Seifert, International Journal of Hydrogen Energy **36**, 6005 (2011).
[14]A. Battisti, S. Taioli, and G. Garberoglio, Microporous and Mesoporous Materials **143**, 46 (2011).
[15]C. Chmelik, D. Freude, H. Bux, and J. Haase, Microporous and Mesoporous Materials **147**, 135 (2012).
[16]H. Bux, C. Chmelik, J. M. van Baten, R. Krishna, and J. Caro, Advanced Materials **22**, 4741 (2010).
[17]H. Wu, W. Zhou, and T. Yildirim, J. Phys. Chem. C **113**, 3029 (2009).
[18]M. Zhou, Q. Wang, L. Zhang, Y.-C. Liu, and Y. Kang, J. Phys. Chem. B **113**, 11049 (2009).
[19]J. Liu, S. Keskin, D. S. Sholl, and J. K. Johnson, J. Phys. Chem. C **115**, 12560 (2011).
[20]H.-C. Guo, F. Shi, Z.-F. Ma, and X.-Q. Liu, J. Phys. Chem. C **114**, 12158 (2010).
[21]S. S. Han, S.-H. Choi, and W. A. Goddard, J. Phys. Chem. C **114**, 12039 (2010).
[22]X.-J. Hou and H. Li, J. Phys. Chem. C **114**, 13501 (2010).
[23]B. Li, S. Wei, and L. Chen, Molecular Simulation **37**, 1131 (2011).
[24]D. Liu, C. Zheng, Q. Yang, and C. Zhong, J. Phys. Chem. C **113**, 5004 (2009).
[25]R. B. Rankin, J. Liu, A. D. Kulkarni, and J. K. Johnson, J. Phys. Chem. C **113**, 16906 (2009).
[26]A. Sirjoosingh, S. Alavi, and T. K. Woo, J. Phys. Chem. C **114**, 2171 (2010).
[27]H. Wu, W. Zhou, and T. Yildirim, J. Amer. Chem. Soc. **129**, 5314 (2007).
[28]M. Dion, H. Rydberg, E. Schröder, D. C. Langreth, and B. I. Lundqvist, Phys. Rev. Lett. **92**, 246401 (2004).
[29]K. Lee, É. D. Murray, L. Kong, B. I. Lundqvist, and D. C. Langreth, Phys. Rev. B **82**, 081101 (2010).
[30]J. Klimeš, D. R. Bowler, and A. Michaelides, J. Phys.: Condensed Matter **22**, 022201 (2010).
[31]J. Klimeš, D. R. Bowler, and A. Michaelides, Phys. Rev. B **83**, 195131 (2011).
[32]G. Román-Pérez and J. M. Soler, Phys. Rev. Lett. **103**, 096102 (2009).
[33]L. Kong, V. R. Cooper, N. Nijem, K. Li, J. Li, Y. J. Chabal, and D. C. Langreth, Phys. Rev. B **79**, 081407 (2009).
[34]L. Kong, G. Román-Pérez, J. M. Soler, and D. C. Langreth, Phys. Rev. Lett. **103**, 096103 (2009).
[35]L. Kong, Y. J. Chabal, and D. C. Langreth, Phys. Rev. B **83**, 121402 (2011).
[36]J. G. Harris and K. H. Yung, J. Phys. Chem. **99**, 12021 (1995).
[37]W. L. Jorgensen and J. Tirado-Rives, J. Amer. Chem. Soc. **110**, 1657 (1988).
[38]Y. Houndonougbo, C. Signer, N. He, K. G. Ray, W. Morris, H. Furukawa, M. Asta, B. Laird, and O. Yaghi (unpublished).
[39]J. P. Perdew, K. Burke, and M. Ernzerhof, Phys. Rev. Lett. **77**, 3865 (1996).
[40]C. Campañá, B. Mussard, and T. K. Woo, J. Chem. Theory Comp. **5**, 2866 (2009).
[41]S. Plimpton, J. Comp. Phys. **117**, 1 (1995); [http://lammps.sandia.gov].
[42]S. J. Plimpton, R. Pollock, and M. Stevens, in *Particle-Mesh Ewald and rRESPA for Parallel Molecular Dynamics Simulations in Proceedings of the Eighth SIAM Conference on Parallel Processing for Scientific Computing, Minneapolis, MN* (Society for Industrial & Applied Mathematics, Philadelphia, PA, 1997).
[43]Y. Zhang and W. Yang, Phys. Rev. Lett. **80**, 890 (1998).
[44]J. P. Perdew and Y. Wang, Phys. Rev. B **33**, 8800 (1986).
[45]A. D. Becke, Phys. Rev. A **38**, 3098 (1988).
[46]G. Kresse and J. Hafner, Phys. Rev. B **47**, RC558 (1993); G. Kresse and J. Hafner, *ibid.* **49**, 14251 (1994); G. Kresse and J. Furthmller, Comp. Mat. Sci. **6**, 15 (1996); G. M. Zhang and A. C. Hewson, Phys. Rev. B **54**, 1169 (1996).
[47]P. E. Blöchl, Phys. Rev. B **50**, 17953 (1994); G. Kresse and D. Joubert, *ibid.* **59**, 1758 (1999).
[48]H. Casimir and D. Polder, Phys. Rev. **73**, 360 (1948).
[49]C. Mavroyannis and M. Stephen, Molecular Physics **5**, 629 (1962).
[50]P. W. Langhoff and M. Karplus, J. Chem. Phys. **53**, 233 (1970).